Free water in white matter differentiates MCI and AD from control subjects

Matthieu Dumont[a,g,1], Maggie Roy[c,a,g], Pierre-Marc Jodoin[b,a,g], Felix C. Morency[a], Jean-Christophe Houde[c,a], Zhiyong Xie[d], Cici Bauer[f], Tarek A. Samad[e], Koene R. A. Van Dijk[d], James A. Goodman[d,h], Maxime Descoteaux[c,a,h]

[a] *Imeka Solutions, Inc, Sherbrooke, QC, Canada*
[b] *VITAlab, University of Sherbrooke, Sherbrooke, QC, Canada*
[c] *SCIL (Sherbrooke Connectivity Imaging Lab), University of Sherbrooke, Sherbrooke, QC, Canada*
[d] *Clinical & Translational Imaging, Pfizer, Inc, Cambridge, MA, United States*
[e] *Internal Medicine Research Unit, Pfizer, Inc, Cambridge, MA, United States*
[f] *Department of Biostatistics and Data Science, The University of Texas Health Science Center at Houston, Houston, TX, United States*
[g] *These first authors contributed equally*
[h] *These senior authors contributed equally*
[i] *Corresponding author: matthieu.dumont@imeka.ca*

Abstract

Recent evidence show that neuroinflammation plays a role in many neurological diseases including mild cognitive impairment (MCI) and Alzheimer's disease (AD), and that free water (FW) modeling from clinically acquired diffusion MRI (DTI-like acquisitions) can be sensitive to this phenomenon. This FW index measures the fraction of the diffusion signal explained by isotropically unconstrained water, as estimated from a bi-tensor model. In this study, we developed a simple FW processing pipeline that uses a safe white matter (WM) mask without gray matter (GM)/CSF partial volume contamination (WM_{safe}) near ventricles and sulci. We investigated if FW inside the WM_{safe} mask, including and excluding areas of white matter damage such as white matter hyperintensities (WMHs) as shown on T2 FLAIR, computed across the whole white matter could be indicative of diagnostic grouping along the AD continuum.

After careful quality control, 81 cognitively normal controls (NC), 103 subjects with MCI and 42 with AD were selected from the ADNIGO and ADNI2 databases. We show that MCI and AD have significantly higher FW measures even after removing all partial volume contamination. We also show, for the first time, that when WMHs are removed from the masks, the significant results are maintained, which demonstrates that the FW measures are not just a byproduct of WMHs. Our new and simple FW measures can be used to increase our understanding of the role of inflammation-associated edema in AD and may aid in the differentiation of healthy subjects from MCI and AD patients.

1. Introduction

White matter (WM) atrophy in Alzheimer's disease (AD) was observed more than three decades ago [1]. The microstrucutural changes observed in the WM of AD patients include axonal deterioration, Wallerian degeneration, loss of myelin density, loss of oligodendrocytes, microglia activation and vascualar degeneration [2, 3, 4, 5, 6, 7]. Numerous studies have shown that changes in the WM are an early event in the development of AD, happening in preclinical stages [3, 8, 9]. Changes in the microstructure of WM have even been reported before measurable hippocampal atrophy in mild cognitive impairment (MCI) [10] and preclinical AD [11]. More recent evidence shows that chronic neuroinflammation also contributes to the process of neurodegeneration in AD and was recently observed in the WM of AD patients [12].

Microglia-induced neuroinflamation in patients have been mostly studied using PET imaging ligands such as 11C-PK11195 [13]. However, to identify WM changes, diffusion MRI has been the modality of choice [14]. Studies, in the past decade, have identified various regions in the WM where the diffusion measures, mostly diffusion tensor imaging (DTI)-based measures such as fractional anisotropy and mean, axial, and radial diffusivities, correlate with symptoms of MCI and AD [15, 16, 17, 18, 19]. A more recent diffusion measure is the free water (FW) index, which measures the fraction of the diffusion signal explained by isotropically unconstrained water [20], as estimated from a regularized bi-tensor model. In white matter, this measurement represents either FW in extracellular space around axons or FW contamination from cerebrospinal fluid in adjacent voxels. An elevated FW index in white matter has been suggested to indicate neuroinflammation [21] and has been described in normal aging [22] and many neurological disorders such as schizophrenia [23, 24, 25], Parkinson's disease [26], and AD [27, 28, 29].

In AD patients, an association between the widespread increased FW and poorer attention, executive functioning, visual construction, and motor performance was shown in [28, 29]. FW-corrected DTI measures are more sensitive to differentiate AD groups compared to standard DTI measures [29]. In a longitudinal study, FW-corrected radial diffusivity, but not un-corrected radial diffusivity, was higher in the WM of MCI patients who converted to AD compared to MCI patients who did not convert [27]. FW-corrected DTI measures also demonstrate greater sensitivity to associations between AD pathology and white matter microstructure compared to standard DTI measures [11].

In this study, we developed a FW processing pipeline that uses a WM *"safe"* mask (WM_{safe}) without GM/CSF partial volume contamination and computed new and simple whole-brain FW measures based on this WM_{safe} mask (including and excluding WMHs within the mask) for three different groups (cognitively normal, MCI and AD subjects), selected from the ADNIGO and ADNI2 databases. The prevalence and degree of WMHs is known to increase with age [30] and therefore WMHs cannot be ignored in WM processing of aged groups. We show that our FW measures were significantly higher in MCI and AD groups compared to NC, but only when using a WM safe mask. We also show, for the first time, that when WMHs are removed from the mask, the significant results remained, which demonstrates that FW measures are not just a byproduct of WMHs.

2. Methods

2.1. Study participants

226 subjects from the ADNIGO and ADNI2 databases passed the necessary quality assurance (QA) phases of the diffusion MRI analysis pipeline (described below). Of those participants, 81 (38 males, 43 females) were cognitively normal (normal control, NC), 103 (69 males, 34 females) had a diagnosis of mild cognitive impairment (MCI) and 42 (25 males, 17 females) had a diagnosis of AD. Age range per group was between 67 and 95 years for NCs, between 60 and 95 years for MCIs and bewteen 61 and 97 for ADs. Mean age was 78.46 for NCs, 79.0 for MCIs and 79.38 for ADs. All participants had good general health, good hearing and seeing abilities, no depression or bipolar condition, no history of alcohol or drug abuse and completed at least six grades of education. Also, NCs had no memory impairment and their clinical dementia rating (CDR) was 0. MCI subjects included early and late MCI with impaired memory and a CDR of 0.5, while AD subjects met criteria for dementia and had a CDR between 0.5 and 1 [31]. Participants did not suffer from any neurological disorders other than MCI and AD such as brain tumor, multiple sclerosis, Parkinson's disease, or traumatic brain injury.

2.2. MRI data acquisition

Data for each participant came from the ADNIGO and ADNI2 databases[1]. Of the available modalities, we used the T1w, diffusion weighted imaging (DWI) and fluid attenuation inversion recovery (FLAIR) scans. The DWI scans were acquired along 41 evenly distributed directions using

[1] http://adni.loni.usc.edu/

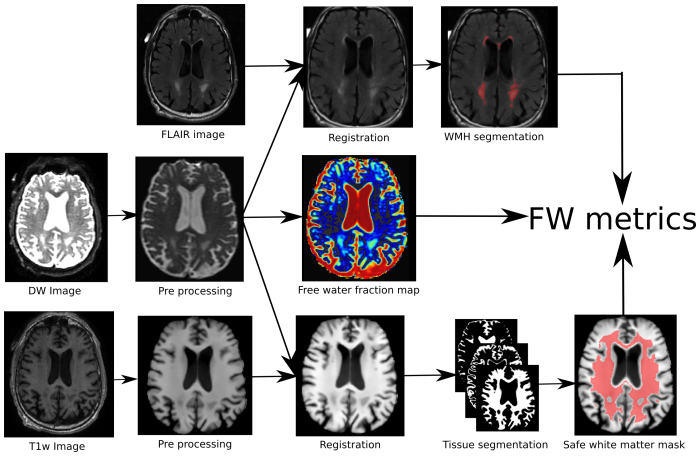

Figure 1: Pipeline of the proposed method: (1) the DWI and T1w images are first preprocessed, (2) the three modalities are co-registered of which (3) are extracted the FW map, the tissue map and the WMHs areas. (4) the combination of the three maps leads to the proposed FW metrics.

a b-value of 1000 s/mm^2 with a $1.3 \times 1.3 \times 2.7$ mm^3 spatial resolution. The T1w and FLAIR scans were acquired at $1.2 \times 1.05 \times 1.05$ and $0.85 \times 0.85 \times 5$ mm^3 spatial resolution, respectively. Data was acquired at 58 different North-American locations.

2.3. MRI processing pipeline

The processing pipeline is illustrated in Figure 1. At first, the T1w and DW images were denoised with a non-local means method robust to Rician noise [32], followed by an MRI bias field correction performed with ANTs N4 correction tool [33]. The brain mask (BM) was then processed and the skull was removed using the BEaST brain extraction software [34]. We referred to these methods as the *preprocessing* step in Figure 1. Then, the T1w and FLAIR images were nonlinearly registered to the 1x1x1 up-sampled diffusion space with ANTs registration [33]. Tissue segmentation was then performed on the transformed T1w to obtain a binary map of the CSF, GM, and WM. This was done using ANTs Atropos [33]. In order to prevent any CSF contamination in regions susceptible to partial volume effect, a "safe WM mask" (WM_{safe}) was built by combining the following morphological operations on the CSF, WM, GM and brain binary masks:

$$WM_{\text{safe}} = ((WM - (GM \oplus R^1)) - (CSF \oplus R^1)) \cap (BM \ominus R^{15}), \tag{1}$$

where R^n is a 3D structuring element of radius n, $\oplus$ is the dilatation operator, $\ominus$ is the erosion operator and $\cap$ the intersection operator as illustrated in Figure 1. Using the FLAIR and T1w images,

a binary map of WMHs was also computed using *volBrain* [35]. The bi-tensor model proposed by Pasternak et al. [20] was fit onto the DW signal. The result of this fit is a fraction representing the contribution of unconstrained water to the original signal and a new signal representing the tissue contribution. The fraction of unconstrained water contribution in a voxel is what we commonly call FW volume and the 3D image of this FW volume is called the FW map. The tissue signal is the FW-corrected DWI signal, as it represents the signal without its unconstrained component. The safe white matter mask, the WMH mask, and the FW map were then used to extract the mean FW value (μFW) and the relative FW volume (rFW). The rFW is the total volume of FW voxels within the safe white matter mask with FW values greater than 0.1, divided by the total volume of the safe white matter mask. rFW_m and μFW_m are defined as such:

$$rFW_m = \frac{volume(FW_m > 0.1)}{volume(m)}, \tag{2}$$

$$\mu FW_m = \overline{FW_m}, \tag{3}$$

where $m \in \{WM_{\text{safe}}, WMHs, WM_{\text{safe}} - WMHs\}$. The 0.1 threshold was chosen to minimize the impact of noise on the rFW metric. All processing was done using a Nextflow [36] pipeline with all software dependencies bundled in a Singularity container [37] ensuring quick and easy reproducibility of the results.

2.4. Statistics

A cross-sectional analysis was performed at the first available time point comparing rFW and μFW in NC (n=81), MCI (n=103), and AD (n=42). An analysis of variance (ANOVA) was performed to test for a main effect of diagnostic group followed by a post-hoc pairwise Tukey test to assess differences between sub groups [38]. A log transformation was applied to the rFW and μFW metrics to improve normality of the distribution before analyses [39].

2.5. Quality assurance

Out of all available subjects in ADNI2 and ADNIGO, 239 had at least one time point with all the images required (T1w, DWI and FLAIR) to go through the processing pipeline. Visual QA was performed on all images of all time points and those with problems impossible to correct (missing brain parts, acquisition artifacts) were rejected. Gradient information was also QA-ed to make sure every DWI image had 41 evenly distributed direction on one single acquisition shell. This first QA

pass eliminated 9 subjects bringing the count of subjects with usable data to 230. Visual inspection was performed on brain extraction of T1w and DWI as well as on the non-linear registration of the FLAIR on the T1w and of the T1w on DWI. Every tissue segmentation mask (WM, GM, CSF) as well as the WMH mask was inspected. This second QA pass eliminated 4 subjects, 3 with artefacts in the DWI images causing improbable values in metrics and one with an obviously incorrect T1 brain mask, leaving 226 subjects with usable data for the group analysis.

3. Results

As shown in Table 1 results of the initial ANOVA tests show a significant main effect of group membership across all regions of interests. Post-hoc Tukey tests show that both rFW and μFW are significantly higher in the WM_{safe} for MCI and AD subjects than for NC subjects whether or not $WMHs$ were included. Interestingly, when looking at rFW and μFW specifically within the WMH mask we do see significant between-group differences but with lesser effect and neither of them being able to separate both NC-MCI and NC-AD.

Table 1: The F-statistic obtained from the ANOVA test is displayed in the first column and the rest of the table shows the Tukey post-hoc pairwise group differences(on log-scale) with the standard error in parentheses. The statistical significance(in bold) is shown as: * p<0.05, ** p<0.01, *** p<0.001.

	F(2, 223)	NC-MCI(SE)	NC-AD(SE)	MCI-AD(SE)
$rFW_{WM_{\text{safe}}-WMHs}$	**16.02*****	**-0.52(0.18)*****	**-0.86(0.23)*****	-0.34(0.20)
$\mu FW_{WM_{\text{safe}}-WMHs}$	**13.58*****	**-0.49(0.17)*****	**-0.70(0.19)*****	-0.21(0.20)
$rFW_{WM_{\text{safe}}}$	**12.79*****	**-0.53(0.19)*****	**-0.90(0.22)*****	–0.36(0.21)
$\mu FW_{WM_{\text{safe}}}$	**12.66*****	**-0.50(0.17)*****	**-0.74(0.20)*****	-0.23(0.20)
rFW_{WMHs}	**4.14***	**-0.13(0.07)***	-0.14(0.10)	-0.01(0.09)
μFW_{WMHs}	**3.80***	-0.13(0.08)	**-0.18(0.10)***	-0.05(0.10)

To represent the spatial differences in free water repartition between groups, every T1W image already registered in diffusion space was non-linearly registered to the MNI152 space with the ANTs registration tool [33]. The resulting transformations were applied to the free water volumes. Mean and standard deviation free water volume for each group was computed and used to obtain a z-score volume of each subject compared to each group. These z-score volumes were averaged and thresholded at z $\geq$ 2 standard deviations to obtain binary group comparison volumes.

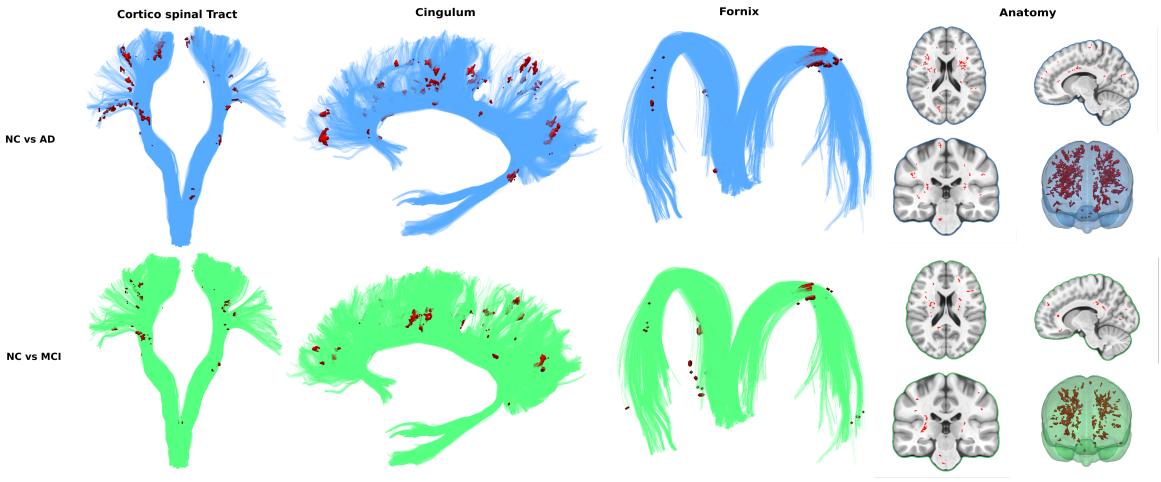

Figure 2: Spatial repartition in free water differences across groups

In both the NC vs AD and NC vs MCI comparisons, the voxels showing differences are mostly located in the corticospinal tract (CST) and bundles of the limbic system such as the cingulum and the fornix. Figure 2 shows that intensity and location of significant z-score clusters is different when comparing AD or MCI to NC.

4. Discussion

We have shown that MCIs and ADs have significantly higher FW metrics compared to NCs. There was a correlation between FW and age but it was found to be weak and consistent across all groups. We also demonstrated that the use of a safe WM mask is critically important to prevent partial volume contamination that can perturb the overall results. Our new and simple FW measures can be used to increase our understanding of the role of inflammation-associated edema in AD and may aid in the differentiation of healthy subjects from MCI and AD patients. Significant results were also obtained when WMHs were removed from the WM mask, which demonstrate that FW metrics differences between group were not due to white matter lesions that can be seen on T2 FLAIR images as WMHs. In fact, a key observation of this study is that FW in MCI and AD subjects is globally distributed through the WM and is not specifically associated to WMHs or other regions typically associated to cognition like the limbic system.

Neither FW metrics could differentiate between MCI and AD subjects. This result could be attributed to the study design since measuring FW metrics in non-specific anatomical brain region

such as the whole WM gives a very broad picture of the FW content in the brain, which may hide localized differences. Analyzing FW content along specific WM bundles would be expected to yield more specific results. To do so, tractography would then be used to reconstruct the global WM architecture followed by an automated segmentation of several key WM bundles such as the fornix, cingulum, corpus callosum, and association tracts (arcuate fasciculus, uncinate, inferior longitudinal and inferior fronto-occipital fasciculus). FW metrics would be analyzed along those bundles, as done in apparent fiber quantification (AFQ) [40] and tract-profiling [41]. Future work would also include looking at how FW correlates with abeta and tau data available in ADNI to further support the hypothesis that FW is a good correlate measurement of neuroinflammation.

However, FW metrics also have limitations, i.e. they are derived from a bi-tensor model, which is limited to representing a FW compartment and a single fiber population. However, it is estimated that 66 to 90 percent of brain WM voxels contain at least two fiber populations [27, 28]. In those voxels, the estimated contribution of the FW compartment is incorrectly estimated, since some signal arising from the fiber populations not fitted to the single fiber tensor will be assigned to the FW compartment. To correct this bias, a FW model accounting for more than one fiber population would need to be used to better fit the signal. While a more sophisticated model would certainly better characterize the information contained in the non-free-water portion of the signal and give more accurate free water indices, these models require multi-shell DWI acquisitions which are unavailable in ADN2 and ADNIGO.

5. Conclusion

This study demonstrates that after removing partial volume contamination as well as WMHs lesions, the free water content of healthy looking white matter differentiates MCI and AD groups from healthy subjects. Our method is based on existing DTI-like diffusion data, is atlas free, requires no registration with a reference brain, no PET scan, no tractography, has few tunable parameters, and takes a few minutes only of computation. The method is a simple but powerful approach that may be used in the context of patient selection and stratification for novel treatments that are aimed at treating or preventing inflammation components of AD using legacy or standard diffusion MRI data. The significant differences of our FW metrics between NC and MCI as well as NC and AD may demonstrate the potential of FW as a tool to study neuroinflammation. We intend to extend this work with analyses of FW metrics in specific white matter bundles and sections of bundles. Also, characterization over time of our new FW metrics in an MCI population could help differentiate

those older adults who will remain relatively stable and those who will progress to AD, which has utility for patient selection and stratification of subjects in preclinical stages of AD.

6. Acknowledgements

This research has been evenly funded by Imeka Solution inc. and Pfizer inc.

7. Disclosure statement

At the time the work was completed, Matthieu Dumont, Maggie Roy, Pierre-Marc Jodoin, Felix C. Morency, Jean-Christophe Houde and Maxime Descoteaux were employees at Imeka solutions inc. and Koene R. A. Van Dijk, Cici Bauer, Zhiyong Xie, Tarek A. Samad, and James Goodman were employees of Pfizer inc. No other potential conflicts of interest were disclosed.

8. References

[1] A. Brun, E. Englund, A white matter disorder in dementia of the Alzheimer type: A pathoanatomical study, Annals of Neurology 19 (3) (1986) 253–262. doi:10.1002/ana.410190306.

[2] A. Brun, E. Englund, Brain changes in dementia of Alzheimer's type relevant to new imaging diagnostic methods, Progress in Neuropsychopharmacology and Biological Psychiatry 10 (3-5) (1986) 297–308. doi:10.1016/0278-5846(86)90009-6.

[3] S. M. de la Monte, Quantitation of cerebral atrophy in preclinical and endstage alzheimer's disease, Annals of Neurology 25 (5) (1989) 450–459. doi:10.1002/ana.410250506.

[4] M. Brilliant, L. Hughes, D. Anderson, M. Ghobrial, R. Elble, Rarefied White Matter in Patients withAlzheimer's, Alzheimer Disease and Associated Disorders 9 (1) (1995) 39–46.

[5] E. Englund, Neuropathology of White Matter Changes in Alzheimer's Disease and Vascular Dementia, Logo Dementia and Geriatric Cognitive Disorders 9 (suppl 1) (1998) 6–12.

[6] J. M. Burns, J. A. Church, D. K. Johnson, C. J. Xiong, D. Marcus, A. F. Fotenos, A. Z. Snyder, J. C. Morris, R. L. Buckner, White matter lesions are prevalent but differentially related with cognition in aging and early Alzheimer disease, Archives of Neurology 62 (12) (2005) 1870–1876. doi:10.1001/archneur.62.12.1870.

[7] M. Sjöbeck, M. Haglund, E. Englund, Decreasing myelin density reflected increasing white matter pathology in azheimer's disease - A neuropathological study, International Journal of Geriatric Psychiatry 20 (10) (2005) 919–926. doi:10.1002/gps.1384.

[8] K. Kantarci, R. Petersen, B. Boeve, D. Knopman, DWI predicts future progression to Alzheimer disease in amnestic mild cognitive impairment, Neurology 64 (June 2000) (2005) 902–904. doi:10.1212/01.WNL.0000153076.46126.E9.DWI.

[9] M. K. Desai, K. L. Sudol, M. C. Janelsins, M. A. Mastrangelo, E. Frazer, W. J. Bowers, Triple-transgenic Alzheimer's disease mice exhibit region- specific abnormalities in brain myelination patterns prior to appearance of amyloid and tau pathology, Glia 57 (1) (2009) 54–65. doi:10.1002/glia.20734.Triple-transgenic.

[10] L. Zhuang, P. S. Sachdev, J. N. Trollor, S. Reppermund, N. A. Kochan, H. Brodaty, W. Wen, Microstructural White Matter Changes, Not Hippocampal Atrophy, Detect Early Amnestic Mild Cognitive Impairment, PLoS ONE 8 (3) (2013) 1–10. doi:10.1371/journal.pone.0058887.

[11] A. R. Hoy, M. Ly, C. M. Carlsson, O. C. Okonkwo, H. Zetterberg, K. Blennow, M. A. Sager, S. Asthana, S. C. Johnson, A. L. Alexander, B. B. Bendlin, Microstructural white matter alterations in preclinical Alzheimer's disease detected using free water elimination diffusion tensor imaging, PLoS ONE 12 (3) (2017) 1–21. doi:10.1371/journal.pone.0173982.

[12] D. Raj, Z. Yin, M. Breur, J. Doorduin, I. R. Holtman, M. Olah, I. J. Mantingh-Otter, D. Van Dam, P. P. De Deyn, W. den Dunnen, et al., Increased white matter inflammation in aging-and alzheimers disease brain, Frontiers in molecular neuroscience 10 (2017) 206.

[13] E. Zimmer, A. Leuzy, A. Benedet, J. Breitner, S. Gauthier, P. Rosa-Neto, Tracking neuroinflammation in Alzheimer's disease: the role of positron emission tomography imaging, Journal of Neuroinflammation 11 (1) (2014) 120. doi:10.1186/1742-2094-11-120.

[14] D. Jones (Ed.), Diffusion MRI: Theory, Methods And Applications, Oxford University Press, 2010.

[15] R. Mito, D. Raffelt, T. Dhollander, D. N. Vaughan, J. D. Tournier, O. Salvado, A. Brodtmann, C. C. Rowe, V. L. Villemagne, A. Connelly, Fibre-specific white matter reductions in Alzheimer's disease and mild cognitive impairment, Brain 141 (3) (2018) 888–902. doi:10.1093/brain/awx355.

[16] G. Stebbins, C. Murphy, Diffusion tensor imaging in alzheimers disease and mild cognitive impairment, Behavioural Neurology 21 (2009) 3949.

[17] S. Galluzzi, M. Marizzoni, C. Babiloni, D. Albani, L. Antelmi, C. Bagnoli, D. Bartres-Faz, S. Cordone, M. Didic, L. Farotti, U. Fiedler, G. Forloni, N. Girtler, T. Hensch, J. Jovicich, A. Leeuwis, C. Marra, J. L. Molinuevo, F. Nobili, J. Pariente, L. Parnetti, P. Payoux, C. Del Percio, J. P. Ranjeva, E. Rolandi, P. M. Rossini, P. Schönknecht, A. Soricelli, M. Tsolaki, P. J. Visser, J. Wiltfang, J. C. Richardson, R. Bordet, O. Blin, G. B. Frisoni, Clinical and biomarker profiling of prodromal Alzheimer's disease in workpackage 5 of the Innovative Medicines Initiative PharmaCog project: A 'European ADNI study', Journal of Internal Medicine 279 (6) (2016) 576–591. doi:10.1111/joim.12482.

[18] M. A. Nowrangi, P. B. Rosenberg, The fornix in mild cognitive impairment and Alzheimer's disease, Frontiers in Aging Neuroscience 7 (JAN) (2015) 1–7. doi:10.3389/fnagi.2015.00001.

[19] C. D. Smith, H. Chebrolu, A. H. Andersen, D. A. Powell, M. A. Lovell, S. Xiong, B. T. Gold, White matter diffusion alterations in normal women at risk of Alzheimer's disease, Neurobiology of Aging 31 (7) (2010) 1122–1131. doi:10.1016/j.neurobiolaging.2008.08.006.

[20] O. Pasternak, N. Sochen, Y. Gur, N. Intrator, Y. Assaf, Free water elimination and mapping from diffusion mri, Magn Reson Med. 62 (3) (2009) 717–730.

[21] O. Pasternak, M. Shenton, C.-F. Westin, Estimation of extracellular volume from regularized multi-shell diffusion mri, Med Image Comput Comput Assist Interv 15 (2) (2012) 305–312.

[22] J. A. Chad, O. Pasternak, D. H. Salat, J. J. Chen, Re-examining age-related differences in white matter microstructure with free-water corrected diffusion tensor imaging, Neurobiology of aging 71 (2018) 161–170.

[23] O. Pasternak, C.-F. Westin, S. Bouix, L. J. Seidman, J. M. Goldstein, T.-U. W. Woo, T. L. Petryshen, R. I. Mesholam-Gately, R. W. McCarley, R. Kikinis, M. E. Shenton, M. Kubicki, Excessive Extracellular Volume Reveals a Neurodegenerative Pattern in Schizophrenia Onset, Journal of Neuroscience 32 (48) (2012) 17365–17372. `arXiv:NIHMS150003`, `doi:10.1523/JNEUROSCI.2904-12.2012`.

[24] O. Pasternak, C.-F. Westin, B. Dahlben, S. Bouix, M. Kubicki, The extent of diffusion mri markers of neuroinflammation and white matter deterioration in chronic schizophrenia, Schizophrenia research 161 (1) (2015) 113–118.

[25] O. Pasternak, M. Kubicki, M. E. Shenton, In vivo imaging of neuroinflammation in schizophrenia, Schizophrenia research 173 (3) (2016) 200–212.

[26] E. Ofori, O. Pasternak, P. Planetta, H.Li, R. Burciu, A. Snyder, S. Lai, M. Okun, D. Vaillancourt, Free-water within the substantia nigra of parkinson's disease., Brain 138 (8) (2015) 23222331.

[27] K. H. Maier-Hein, C.-F. Westin, M. E. Shenton, M. W. Weiner, A. Raj, P. Thomann, R. Kikinis, B. Stieltjes, O. Pasternak, Widespread white matter degeneration preceding the onset of dementia, Alzheimer's & Dementia 11 (5) (2015) 485–493.

[28] V. Montal, E. Vilaplana, D. Alcolea, J. Pegueroles, O. Pasternak, S. González-Ortiz, J. Clarimón, M. Carmona-Iragui, I. Illán-Gala, E. Morenas-Rodríguez, et al., Cortical microstructural changes along the alzheimer's disease continuum, Alzheimer's & Dementia 14 (3) (2018) 340–351.

[29] F. Ji, O. Pasternak, S. Liu, Y. M. Loke, B. L. Choo, S. Hilal, X. Xu, M. K. Ikram, N. Venketasubramanian, C. L. H. Chen, J. Zhou, Distinct white matter microstructural abnormalities and extracellular water increases relate to cognitive impairment in Alzheimer's disease with and without cerebrovascular disease, Alzheimer's Research and Therapy 9 (1) (2017) 1–10. `doi:10.1186/s13195-017-0292-4`.

[30] M. B. F-E de Leeuw, J C de Groot, E Achten, MOudkerk, LMP Ramos, R Heijboer, A Hofman, J Jolles, J van Gijn, Prevalence of cerebral white matter lesions in elderly people: a population based magnetic resonance imaging study: the Rotterdam Scan Study, Journal of neurology, neurosurgery, and psychiatry 70 (1) (2001) 9–14. `doi:10.1136/jnnp.70.1.2`.

[31] R. C. Petersen, P. Aisen, L. Beckett, M. Donohue, A. Gamst, D. Harvey, C. Jack, W. Jagust, L. Shaw, A. Toga, et al., Alzheimer's disease neuroimaging initiative (adni): clinical characterization, Neurology 74 (3) (2010) 201–209.

[32] M. Descoteaux, N. Wiest-Daesslé, S. Prima, C. Barillot, R. Deriche, Impact of rician adapted non-local means filtering on hardi, in: International Conference on Medical Image Computing and Computer-Assisted Intervention, Springer, 2008, pp. 122–130.

[33] B. B. Avants, N. Tustison, G. Song, Advanced normalization tools (ants), Insight j 2 (2009) 1–35.

[34] S. F. Eskildsen, P. Coupé, V. Fonov, J. V. Manjón, K. K. Leung, N. Guizard, S. N. Wassef, L. R. Østergaard, D. L. Collins, A. D. N. Initiative, et al., Beast: brain extraction based on nonlocal segmentation technique, NeuroImage 59 (3) (2012) 2362–2373.

[35] J. V. Manjón, P. Coupé, volbrain: An online mri brain volumetry system, Frontiers in neuroinformatics 10 (2016) 30.

[36] P. D. Tommaso, M. Chatzou, E. Floden, P. Barja, E. Palumbo, C. Notredame, Nextflow enables reproducible computational workflows, Nature Biotechnology 35 (4) (2017) 316319.

[37] G. Kurtzer, V. Sochat, M. Bauer, Singularity: Scientific containers for mobility of compute, PLoS ONE 12 (5).

[38] J. McDonald, Handbook of Biological Statistics, Sparky House Publishing, 2006.

[39] M. M. Zeineh, Y. Chen, H. H. Kitzler, R. Hammond, H. Vogel, B. K. Rutt, Activated iron-containing microglia in the human hippocampus identified by magnetic resonance imaging in alzheimer disease, Neurobiology of aging 36 (9) (2015) 2483–2500.

[40] J. D. Yeatman, R. F. Dougherty, N. J. Myall, B. A. Wandell, H. M. Feldman, Tract profiles of white matter properties: automating fiber-tract quantification, PloS one 7 (11) (2012) e49790.

[41] M. Cousineau, P.-M. Jodoin, E. Garyfallidis, M.-A. Côté, F. C. Morency, V. Rozanski, M. GrandMaison, B. J. Bedell, M. Descoteaux, A test-retest study on parkinson's ppmi dataset yields statistically significant white matter fascicles, NeuroImage: Clinical 16 (2017) 222–233.